Some design considerations for a Moon-based radio telescope operating at frequencies below 10 MHz

Graham Woan

Mullard Radio Astronomy Observatory

Cavendish Laboratory, Madingley Road, Cambridge, CB3 0HE, UK

March 24, 1997

Contents

1 Scattering effects in turbulent plasmas

1.1 Angular broadening

Low-frequency radio astronomy demands a careful consideration of the effects on the observations of various turbulent plasmas, notably the ionosphere, the interplanetary medium and the interstellar medium. At frequencies well above their plasma frequencies density fluctuations in the plasmas lead to variations in refractive index that scale as the wavelength squared, so the effects are most severe at the lowest frequencies.

In general, a region of space in which the electron density deviates by $\Delta N_{\rm e}$ from the mean gives rise to a change in refractive index of

$$\Delta\eta = -\frac{r_{\rm e}}{2\pi}\lambda^2\Delta N_{\rm e}\,, \tag{1}$$

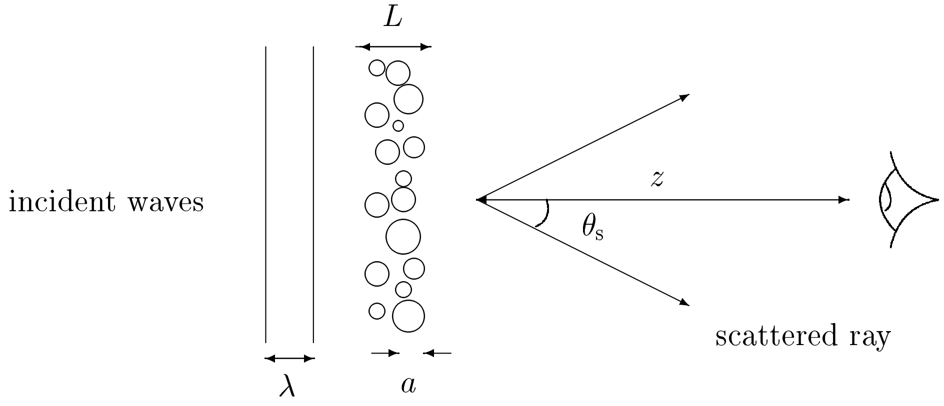

Figure 1: Geometry of the Gaussian 'thin screen' model.

where r_e is the classical radius of an electron (2.82×10^{-15} m) and λ the wavelength of the radiation. To see how this affects radio propagation it is useful to imagine all the density fluctuations from an extended region of space to be compressed to a 'thin screen' of thickness L at some distance z along the line of sight to the radio source (Figure 1). We may further simplify the model by assuming a scale-size of a for the density inhomogeneities (or *blobs*, from now on). This is the so-called 'Gaussian thin-screen model' and displays all the major functional relationships between the radio waves and the plasma.

We see that there is there is an excess change of phase, $\Delta\phi$, of $2\pi\Delta\eta a/\lambda = r_e\lambda a\Delta N_e$ through each blob relative to the free-space path, and each part of the wavefront incident on the thin screen encounters about L/a blobs. If the blobs are arranged randomly this introduces phase fluctuations of

$$\begin{aligned} \Delta\phi_{\rm rms} &= \sqrt{\frac{L}{a}} r_e\lambda a\,\Delta N_e \\ &= r_e\lambda\,\Delta N_e\sqrt{La} \end{aligned} \tag{2}$$

over the screen by the time the wavefront has emerged. At frequencies below 10 MHz we expect the magnitude of these phase fluctuations to be large in the interstellar and interplanetary medium ($\Delta\phi \gg 1$) so the effect is one of a random assembly of small prisms, each deflecting the radiation over a characteristic angle

$$\theta_s = \frac{\lambda\Delta\phi}{2\pi a}. \tag{3}$$

This 'strong scattering' therefore spreads the radiation from a point source over a solid angle of characteristic width

$$\theta_{\mathrm{s}} = \frac{r_{\mathrm{e}}}{2\pi}\lambda^2 \Delta N_{\mathrm{e}} \sqrt{\frac{L}{a}} . \tag{4}$$

A possibly more realistic model uses a Kolmogorov power law for the spatial spectrum of the density fluctuations rather than a fixed scale-size, a. This results a similar relation but with $\theta_{\mathrm{s}} \propto \lambda^{2.2}$ rather than λ^2. The result can be usefully expressed in terms of the integral of the 'turbulence strength' of the medium, C_N^2, along the line-of-sight to the source. This gives a scattering angle of

$$\theta_{\mathrm{s}} \simeq 4.1 \times 10^{-13} \left(\int C_N^2(x)\, dx \right)^{0.6} \lambda^{2.2} \text{ arcsec.} \tag{5}$$

Once we are outside the Earth's ionosphere, the two most important plasma regions that affect radio propagation are the interplanetary medium (IPM) and the interstellar medium (ISM). Both have been observed extensively at decimetre wavelengths (e.g., [1],[4], [8]), allowing us to calibrate the above expressions for θ_{s}.

Under the conditions of strong scattering that we expect at dec<u>a</u>metric wavelengths and longer (i.e., below 30 MHz) we have:

mode	θ_{s}
interplanetary scattering	$\sim 100/(P\nu_{\mathrm{MHz}})^2$ arcmin
interstellar scattering	$\sim 22/\nu_{\mathrm{MHz}}^2$ arcmin

,

where P is the 'impact parameter' of the line of sight to the source relative to the Sun in AU (i.e., about 1). Again we use the Gaussian model, but the two models (Gaussian and Kolmogorov) give roughly similar results over the frequency range considered. We see from this that interplanetary scattering dominates over interstellar scattering by a factor of about 4 (Figure 2). Although interplanetary scattering changes with the solar elongation, most of the material that contributes to the scattering process is within about 1 AU of the Earth and can therefore be thought of as 'local'. The result is that interplanetary scattering does not vary greatly for elongations of more than about 90 degrees.

1.2 Temporal broadening

The scattered rays that broaden the angular size of a point source also give rise to *temporal broadening*. This arises from the range of propagation paths,

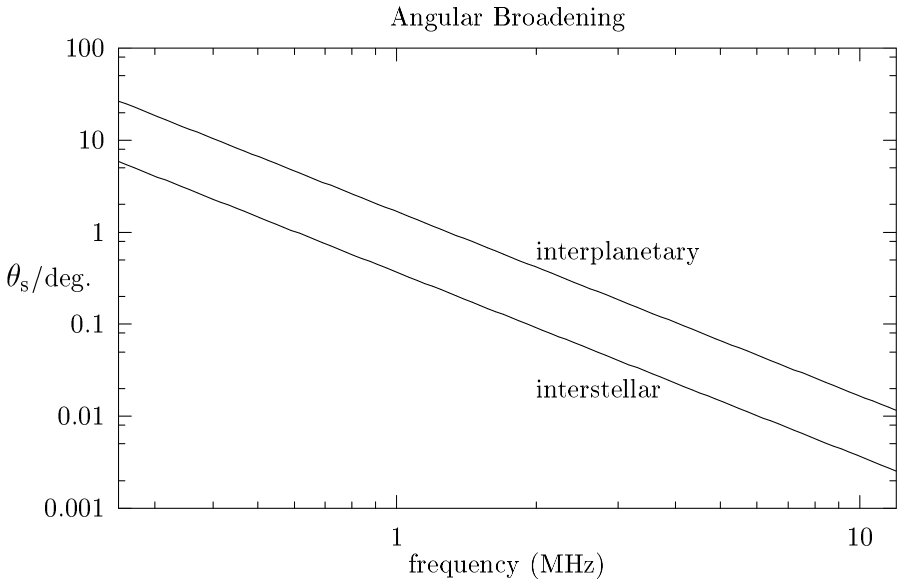

Figure 2: Interplanetary and interstellar angular broadening (Gaussian model).

and hence times, available between the source and the receiver, and will smear transient signals such as pulses from pulsars.

Small-angle approximations give the range in differential propagation times from a source at infinity, broadened to an angular extent of θ_s radians, as approximately

$$\Delta\tau_b = \frac{z\theta_s^2}{2c}\,, \tag{6}$$

where z is the distance between the screen and the observer and c is the speed of light. For a screen at some distance z' from the source the expression is modified by using the *reduced distance*, $z^* = zz'/(z+z')$, in place of z.

Again, this expression can be given an approximate calibration using observations of pulsars and angular broadening at frequencies of a few tens of megahertz [2], to give

mode	$\Delta\tau_b$
interplanetary scattering	$0.1\,\nu_{\mathrm{MHz}}^{-4.4}$ sec
interstellar scattering	$2 \times 10^8 \nu_{\mathrm{MHz}}^{-4.4}$ sec

,

using this time the Kolmogorov model ($\theta_s \propto \nu^{-2.2}$). The two relationships are shown graphically in Figure 3. We see that the vast distances involved in interstellar propagation make the effects of interstellar temporal broadening severe. At 1 MHz the temporal broadening is approximately equal to the proposed mission lifetime of 5 years. Clearly little, if any, temporal work can be done with extra-solar system objects at frequencies below 10 MHz. It is relevant to note that there are only three known pulsars that would *not* be smeared out in this way at 10 MHz.

Interplanetary temporal broadening is less severe, amounting to about 0.1 sec at 1 MHz and 10 sec at 300 kHz. At still lower frequencies we cannot justify the small angle approximation involved in deriving Equation (6), but the effects of this are not too great—at 100 kHz the true temporal broadening is only about a factor of three less than that predicted by Equation (6).

1.3 Faraday rotation

The plane of polarisation of a wave propagating through a plasma will rotate due to 'Faraday rotation' if there is a magnetic field component, $B_{/\!/}$, parallel to the direction of propagation. Explicitly,

$$\mathrm{FR} = \frac{2.36 \times 10^4}{\nu^2} \int N_{\mathrm{e}} B_{/\!/} \, dl \quad \text{radians,} \tag{7}$$

where ν is in Hz, N_{e} in m^{-3} and l in m. Within the solar system both N_{e} (from the solar wind) and B (also from the Sun) drop as $\sim 1/r^2$, so that the Faraday rotation is dominated by the near-Earth environment, giving

$$\mathrm{FR} \simeq \frac{36}{\nu_{\mathrm{MHz}}^2} \quad \text{radians,} \tag{8}$$

(this assumes $B \simeq 6 \times 10^{-9}$ tesla and $N_{\mathrm{e}} \simeq 6.5 \times 10^6\,\mathrm{m}^{-3}$). Both N_{e} and B are highly variable quantities within the solar system, each changing by factors of 3 or 4 on time-scales of hours. This means that polarisation angle is poorly defined at these frequencies, although dual-frequency measurements may go some way to 'unwind' the rotation introduced at the higher frequency ranges.

On the other hand, circular polarisation remains well defined, the only effect of the intervening plasma being the introduction of a phase-lag between the two polarisation components. In the universe as a whole, circular polarisation is rarely seen. This is probably because the radiation mechanisms that generate it (mostly cyclotron processes) are not sufficiently energetic to produce bright sources. The more lunimous synchrotron emission is therefore the dominant mechanism. Within the solar system circularly polarised cyclotron emission from the Sun and planets can be detected, notably from Jupiter and Saturn, and this represents the clearest reason to include a polarisation measuring capability in the VLFA.

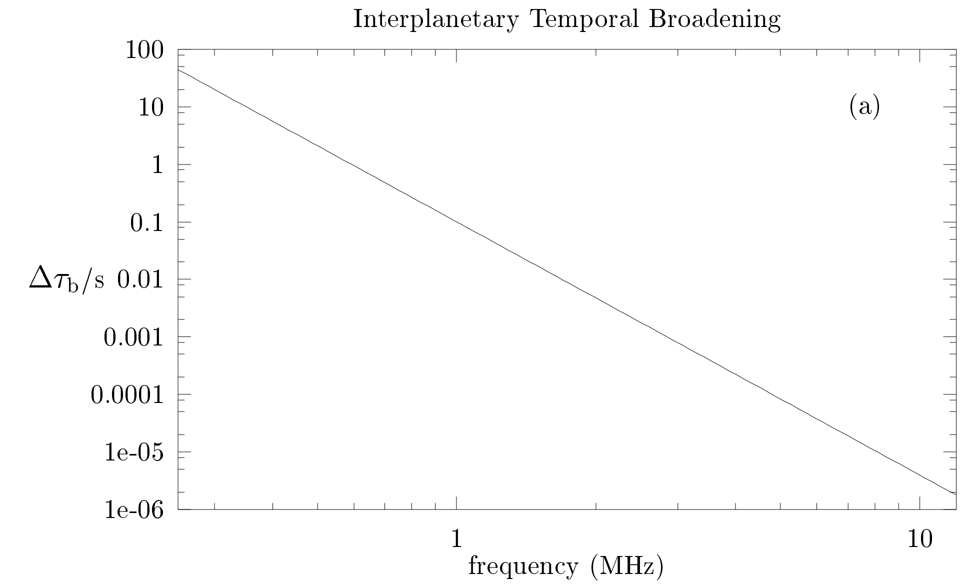

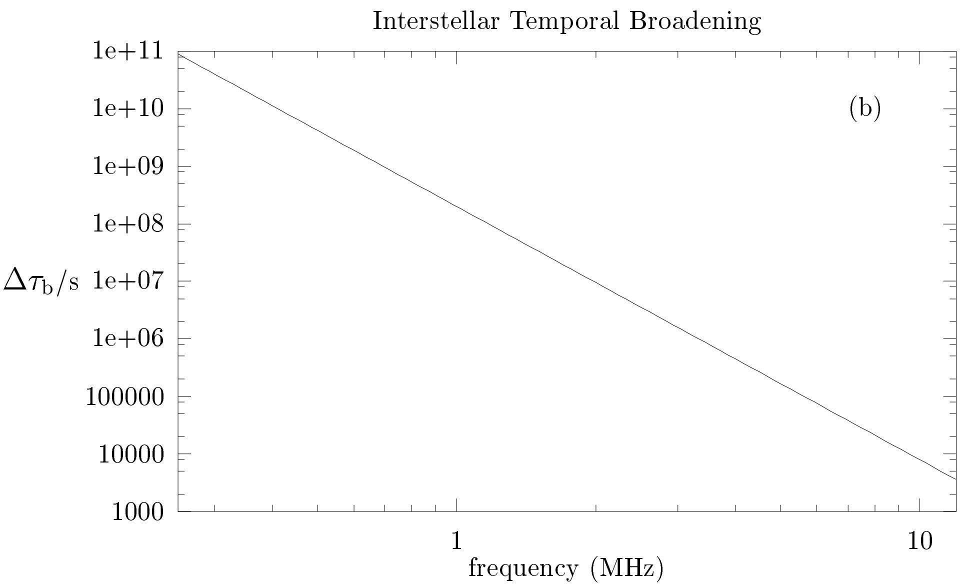

Figure 3: Interplanetary (a) and interstellar (b) temporal broadening (Kolmogorov model).

1.4 Faraday depolarisation

The radiation from a source can travel to the observer over a multiplicity of paths, each with its own, possibly different, Faraday rotation. This gives rise to (linear) Faraday depolarisation, which may be significant within the solar system at very low frequencies. Its effects within the solar system can again be approximated using the Gaussian thin screen-model for the interplanetary medium. From Equation (7) we see that each blob (scale-size a) in the screen (thickness L) will introduce a differential rotation of

$$\Delta\psi = \alpha \Delta N_{\mathrm{e}} \lambda^2 a B_{//}, \tag{9}$$

where $\alpha = 2.6 \times 10^{-13}$ (assuming SI units). The analysis proceeds in a manner similar to that for angular broadening. The wavefront encounters about L/a blobs during its passage through the screen, giving the emerging wavefront a random polarisation structure with an rms polarisation angle of

$$\Delta\psi_{\mathrm{rms}} = \alpha \Delta N_{\mathrm{e}} \lambda^2 a B_{//} \sqrt{\frac{L}{a}}. \tag{10}$$

This can be combined with Equation (4) to give an expression in terms of scattering angle:

$$\Delta\psi_{\mathrm{rms}} = \frac{2\pi\alpha}{r_{\mathrm{e}}} a B_{//} \theta_{\mathrm{s}}. \tag{11}$$

Taking a to be about 200 km for the IPM gives

$$\Delta\psi_{\mathrm{rms}} \simeq \frac{10^{-2}}{\nu_{\mathrm{MHz}}^2}. \tag{12}$$

Although not significant at frequencies greater than about 1 MHz this could be a limiting factor for linear polarisation measurements within the solar system at the lowest reaches of the VLFA frequency range. Furthermore it represents a fundamental limit to linear polarisation measurements as, unlike simple rotation, it cannot be removed by making dual-frequency observations. Circular polarisation is not affected by this process, so the circularly polarised emission from planets will be still be seen, although it will be diluted somewhat by unpolarised background emission.

On the larger scale, we do not expect to see any linear polarisation from galactic or extragalactic signals. Both the amount of rotation and the degree of depolarisation scale as λ^2 at low frequencies [10]. If we take the galactic electron number density to be about 0.3×10^5 m^{-3} and the magnetic field about 5×10^{-10} T, a rotation of 1 radian would be seen over a plasma blob of size $\sim 10^{-3}$ pc at 3 MHz. As we can expect many such blobs within the telescope beam for all but the closest sources, the radiation can be expected to be linearly unpolarised. Furthermore, the total Faraday rotation over interstellar distances is large, amounting to about 10^4 radians per parsec at 1 MHz and scaling as λ^2. The *differential* rotation over the observing band is therefore correspondingly great. At 3 MHz, the differential rotation amounts to 1 radian over a 1 kHz bandwidth after only 0.4 pc.

Any *circularly* polarised signals would preserve their intrinsic degree of polarisation, but as has been mentioned such sources are rare and dim. Unpolarised galactic background emission would add in to reduce the overall degree of polarisation and make detection difficult. There is therefore no reason to expect the detection of extra solar system polarisation of any kind.

The cost of adding a dual polarisation capability to the VLFA is large and the benefit small. It's only use would be for solar-system work that could be done better and more cheaply using in situ spaceraft, so on balance it cannot be recommended.

1.5 Overcoming the scattering limit

The above discussions have assumed that scattering defines a fundamental limit to the angular resolution of a radio telescope operating at frequencies well below 10 MHz. However, the 'image' of a strongly scattered source is *not* a smooth, quasi-Gaussian disc but rather a sequence of overlapping and rapidly changing, narrow-band speckle-patterns. In practice the observing bandwidth and integration time are such that the sum of these patterns is usually seen as a smooth disc. The question arises whether careful measurement of the pattern could be used to reconstruct an undistorted image of the radio source. The analogy is to the de-twinkling of stars by closure phase methods or the phase-correction of radio telescopes by self-calibration algorithms. Although the scattering is strong and in the far-field, there is evidence that reconstructions of this sort could be carried out if speckle measurements could be made sufficiently quickly [3]. We will therefore consider if such measurements are feasible with the VLFA.

Plane waves shining through a thin, strongly scattering screen will give rise to a pattern of intensity fluctuations on the ground with a coherence length of $l_\mathrm{c} = \lambda/\theta_\mathrm{s}$, where θ_s is (again) the angular broadening of the source due to the screen. If the screen is moving perpendicular to the line of sight at a speed v_s then the speckle pattern moves over the observer at the same speed, giving a scintillation time constant of

$$\tau_\mathrm{s} \simeq \frac{l_\mathrm{c}}{v_\mathrm{s}} \simeq \frac{\lambda}{\theta_\mathrm{s} v_\mathrm{s}}. \tag{13}$$

By calibrating from higher frequency measurements, using $\theta_s \propto \lambda^{2.2}$, we get

mode	τ_s
interplanetary scattering	$1.5 \times 10^{-3} \nu_{\mathrm{MHz}}^{1.2}$ sec
interstellar scattering	$44 \times 10^{-3} \nu_{\mathrm{MHz}}^{1.2}$ sec

.

Both forms of scintillation are on a time-scale of milliseconds at frequencies around 1MHz. To see the scintillation, the telescope would therefore need temporal resolution on this time-scale or better.

As well as evolving rapidly in time, the pattern is also a narrow-band phenomenon and would not be seen with a broad-band receiver. If the scattering screen is a distance z away from the observer, signals scattered from the screen at an angle θ_s interfere with the straight-through signal with a phase delay of

$$\phi \simeq \pi \frac{\nu}{c} \theta_s^2 \tag{14}$$

and build up a speckle pattern. A different pattern will be seen if the frequency changes by about $\Delta\nu = c/(z\theta_s^2)$, so this defines the bandwidth of the pattern. Calibrating form observations at higher frequencies we get

mode	$\Delta\nu$
interplanetary scattering	$10\, \nu_{\mathrm{MHz}}^{4.4}$ Hz
interstellar scattering	$5 \times 10^{-9} \nu_{\mathrm{MHz}}^{4.4}$ Hz

.

This indicates that the scintillation bandwidth for ISS is too narrow to be measured realistically, but that interplanetary scintillation could be detected.

There is however a more fundamental limit to the measurement of scintillation. Both the bandwidth and integration time are limited by the above effects. There therefore comes a point at which the product $\tau_s\Delta\nu$ is less that 1, i.e., when no data is available for measurement. Combining Equation(13) with the expression for scintillation bandwidth gives

mode	$\tau_s\Delta\nu$	ν_c
IPS	$1.5 \times 10^{-2} \nu_{\mathrm{MHz}}^{5.6}$ Hz	2.12 MHz
ISS	$2.2 \times 10^{-10} \nu_{\mathrm{MHz}}^{5.6}$ Hz	53 MHz

.

Here ν_c is the critical frequency at which $\tau_s\Delta\nu = 1$ and corresponds to the frequency at which measurements become impossible.

It is clear from this analysis that there is no true diffractive interstellar scintillation at low frequencies and that we cannot, even in principle, remove the effects of the ISM. At frequencies above about 2 MHz however, interplanetary scintillation becomes measurable so that something could be done about the interplanetary medium. For example, interplanetary scintillation could be measured at 5 MHz using a bandwidth of < 10 kHz and an integration time of < 0.01 sec. Bandwidths even narrower than should be available, as they are a natural consequence of a correlation technique that avoids the need for path compensation (see Section 5.2).

Although promising, this technique only becomes viable around the middle of the design frequency range of the VLFA where planetary observations are at their least interesting and it is likely to be computationally awkward for mapping extended structure such as the galactic background. It is therefore not recommended as a processing route unless there is some very pressing need for the slight resolution improvement it would give.

2 Absorption effects

One of the more important effects of the interstellar medium on observations at frequencies below about 10 MHz is the amount of energy transferred from the radiation field to the plasma via charge-separation. This is 'free-free', or 'thermal bremsstrahlung' absorption, and it makes the ionised interstellar medium optically thick (optical depth, τ, of 1) at some frequency ν_{T}. This turnover frequency depends on both the emission measure of the medium and its electron temperature. Specifically,

$$\nu_{\mathrm{T}} = 0.3\, T_{\mathrm{e}}^{0.68} (\underbrace{\int N_{\mathrm{e}}^2\, dx}_{\text{emission measure}})^{1/2} \;\; \mathrm{GHz} \tag{15}$$

at low frequencies, where x is in parsecs along the line-of-sight. Note that this expression assumes the temperature to be constant in the region of interest. The diffuse, warm, interstellar medium has $T_{\mathrm{e}} \simeq 10^4$ K and $N_{\mathrm{e}} \simeq 10^5\ \mathrm{m}^{-3}$. This gives an approximate measure of the distance one can see through the medium before $\tau = 1$. As a function of frequency it is

$$l \simeq (50\nu_{\mathrm{MHz}})^2 \text{ parsec.} \tag{16}$$

This equation is of particular importance in both low-frequency extra-solar system planet searches and extragalactic observations. The galactic disc has a thickness of ~ 1 kpc so that the sky appears uniformly 'foggy' at frequencies below 1–2 MHz [7]. Figure 4 shows an estimate for the visible

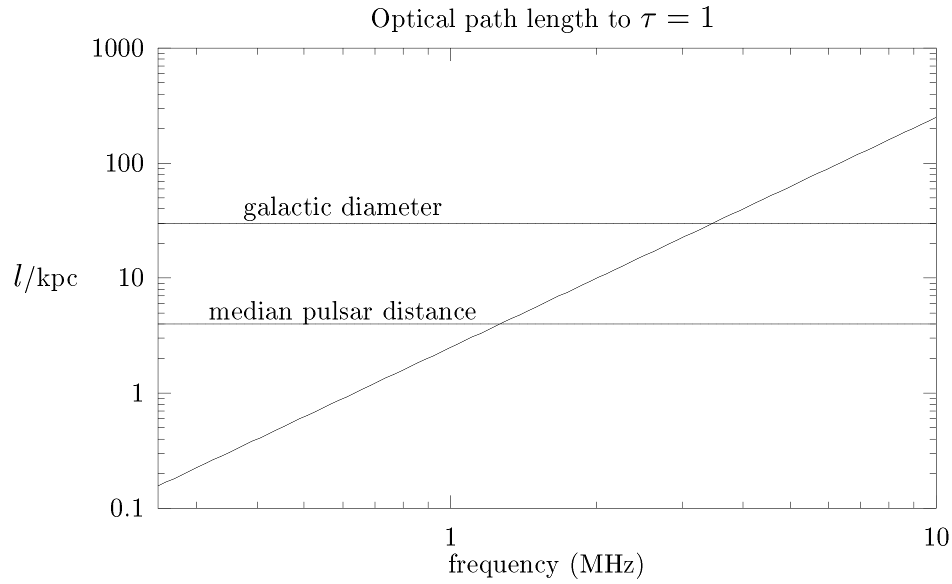

Figure 4: Range of visibility through a uniform interstellar medium as a function of frequency.

optical path length through the IPM as a function of frequency, together with an indication of the median pulsar distance and the galactic diameter. At higher frequencies however, we can see out of the plane, and the plane itself will appear mottled due to the presence of discrete regions of particularly high electron density (H II regions) absorbing the background synchrotron radiation.

At very low frequencies the free-free process absorbs much of the bright background synchrotron emission from the galaxy before it reaches us, causing the system temperature to *decrease*. Observations by the RAE2 spacecraft predict the following antenna temperatures, T_A, as a function of observing frequency, ν, [6]:

T_A (K)	ν (MHz)
3×10^5	10
2×10^6	5
2×10^7	1
2.6×10^7	0.5
5×10^6	0.25

.

Of course, any absorption of this sort will limit the usefulness of the instrument for extra-solar system observations, both because the sky fogs over at some distance, and because the extinction will vary across the sky. This variation will give rise to uncertainties in intrinsic flux density similar to interstellar reddening seen at optical wavelengths. However, it does allow us to study in some detail the distribution of both ionised material and synchrotron emission throughout the galaxy, which is an important field in itself.

3 Investigating the interstellar medium

A good understanding of the interstellar medium is central to the planning and interpretation of radio observations below about 10 MHz. The effects of interstellar scattering have already been considered, but the ISM is in itself one of the major science targets for the VLFA mission.

Generally, the ionised hydrogen seen in the galaxy at low frequencies can be divided into H II regions (often seen as discrete photo-ionised clouds, mostly in the galactic plane) and warm, diffuse gas permeating the plane and extending into the halo. The denser H II regions become optically thick at about 30 MHz due to free-free absorption, whereas the diffuse emission becomes thick at 1–5 MHz [7]. The background synchrotron emission, and the radiation from discrete background sources, is therefore seen against a complex absorption pattern generated by the ISM. This pattern is overlayed with further foreground synchrotron emission to build up an even more complex picture of absorption and emission over the sky.

One task of the VLFA is to disentangle the various components contributing to the observed temperature distribution over the sky. This process relies on both the frequency dependence of these contributions and their analysis in conjunction with ground-based observations. Although the procedure is necessarily quite involved, it is instructive at this stage to consider the major contributing effects, and determine how they might be identified and measured.

Galactic synchrotron emission As the dominant radiation mechanism in the galaxy at these frequencies, most of the radiation the VLFA detects will be galactic synchrotron emission modulated by interstellar absorption. At about 50 MHz the brightness temperature of this emission scales as $\nu^{-2.4}$. This intrinsic spectral index shows some further flattening at lower frequencies before the effects of free-free absorption increase the apparent index to about -1.3 or more at frequencies below 4 MHz. One of the goals of the VLFA will be to determine the value and distribution of the intrinsic synchrotron index over the sky as part of the investigation of the interstellar medium.

Extragalactic radio sources As has already been stated, free-free emission modulates our measurements of intrinsic sky brightness and the flux densities of discrete extragalactic radio sources. The optical depth (c.f. Equation (15)) is

$$\tau \propto T_{\mathrm{e}}^{-1.35} \nu^{-2.1} \int N_{\mathrm{e}}^{2} \, dx \,, \tag{17}$$

assuming the temperature is constant through the integration path. The apparent spectral indices of sources will therefore depend on their intrinsic indices, the emission measure and the electron temperature along their line-of-sight. Each source will also show a spectral turnover at a frequency ν_T due to synchrotron self-absorption ($\nu_{\mathrm{T}} \propto SB^{0.2}/\theta^{2}$) and the Razin-Tsytovič effect ($\nu_{\mathrm{T}} \propto N_{\mathrm{e}}/B$), where B and N_{e} are the magnetic field and electron density local to the source, S its flux density and θ its intrinsic angular size. There are clearly many contributions to the apparent flux density of any single source, and much of the interpretation from discrete sources will therefore be statistical in nature.

Pulsars As has already been discussed, temporal broadening prevents the VLFA from measure pulsar dispersion, but ground-based observations at frequencies > 20 MHz are routine. The dispersion

$$\frac{\partial \tau}{\partial \nu} \propto \nu^{-3} \int N_{\mathrm{e}} \, dx \,, \tag{18}$$

determines the *dispersion measure* (the integral in the above equation) to the pulsar. This can be combined with the emission measure determined from free-free absorption observations to give some indication of the spatial distribution of N_e along the line-of-sight.

Optical line emission Hydrogen recombination (Hα) emission is also of great use in disentangling the various contributing factors to sky brightness. In regions of the sky that are optically thin to Hα (latitudes $\gtrsim 10$ degrees), the emission brightness is proportional to $\int T_{\mathrm{e}}^{-0.92} N_{\mathrm{e}}^{2} \, dx$. H$\alpha$ emission therefore also depends on emission measure but with a slightly different weighting from the electron temperature as compared to free-free absorption. The two can therefore be used for mutual verification in region of the sky optically thin to Hα.

Although the resolution of the telescope will generally be insufficient to measure angular broadening, there should be regions of the sky where this is possible at the lower frequencies. If a sufficient number of background sources exist in these regions, the degree of broadening for each can be used to map the local ISM turbulence strength. This is similar to the approach used successfully to map density structures in the heliosphere using IPS. In principle low frequency observations of this sort are a very sensitive way of measuring weak density structures, as the angular broadening for a given turbulence strength scales as $\lambda^{11/5}$. In practice however it may prove difficult to detect enough background sources in the field of interest and the small variations in angle of scatter may be swamped by the more powerful general structure.

4 Electrical properties of the Moon

A Moon-based low-frequency radio telescope has two basic advantages over one situated on the Earth. Firstly, it does not have to look through the Earth's ionosphere. Secondly, it is shielded from Earth-based radio frequency interference. This second advantage was graphically demonstrated in 1972 by the RAE2 lunar satellite, showing there to be no detectable RFI from the Earth (including auroral emission) on the far-side of the Moon. The first advantage is self evident, but it reminds us that we must consider the effects of the Moon's own atmosphere and, in particular, its ionosphere.

4.1 The lunar ionosphere

The Moon is known to have a tenuous atmosphere, consisting of intrinsic gaseous emission from radioactive decay (mostly ^{40}Ar), captured solar wind and material sputtered from the regolith by energetic particles. However the total mass is thought to be only about 10^4 kg [5]. Although thin, this atmosphere is still capable of having a surprisingly high plasma frequency. If we were to take the entire mass to be ionised hydrogen with a scale-height of 100 km, it would have a plasma frequency of over 12 MHz—similar to that of the Earth. The true ionised fraction and scale-height are therefore of great importance to the viability of a low-frequency instrument on the Moon's surface.

The only direct observations of the ionised component of the lunar atmosphere (other than occultation experiments from Earth) were made by the Luna 19 and 20 probes in the 1970's ([11], [9], [12]). These spacecraft made dual-frequency phase-lag measurements through the atmosphere as they or-

Figure 5: Derived lunar ionosphere densities as a function of altitude (Luna spacecraft observations).

bited the Moon. By fitting these data to a model of the Moon's atmosphere, the electron density in the atmosphere can be estimated as a function of height above the lunar surface. The results vary quite widely, depending on conditions, but show densities of up to 2×10^3 cm^{-3} at altitudes of 2–10 km on the sunlit side (Figure 5). On the dark side of the Moon there is very little ionisation, confirming the idea that the lunar ionosphere, like that of the Earth, is photo-ionised. The densities on the sunlit side are not trivial however, and correspond to plasma frequencies of about 0.5 MHz*.

It appears therefore that, on the sunlit side of the Moon, the ionosphere could prevent measurements at frequencies below 1 MHz. Even at higher frequencies the refractive effects of the ionosphere may cause problems. Observations should therefore be carried out during the lunar night when the ionosphere is at its thinnest and the interference from solar emission is also less. It should be noted here that no reliable measurements of the ionosphere have been carried out at altitudes lower than one or two kilometres, and little has been done on the containing effects of the Moon's own weak magnetic

*To a good approximation, the plasma frequency in MHz of an electron gas of density n cm^{-3} is $\nu_p \simeq \sqrt{n}/100$.

field. A fuller understanding would clearly be needed before the construction of a lunar radio telescope.

4.2 The lunar regolith

The electrical properties of the surface of the Moon are of great importance in the VLFA design. Unlike the Earth, the Moon's surface has a very low electrical conductivity (about $10^{-14}\,\Omega^{-1}\mathrm{m}^{-1}$ at d.c.). This means that we may contemplate receiving the component of the electric field parallel to the surface of the Moon close to its surface. On the Earth this component is largely nulled by a strong surface reflection, π out of phase with the incident wave. Clearly, any radio source high in the sky will illuminate the Moon primarily with this component, so in practice we can expect it to be stronger than the perpendicular component. Furthermore, the receiving elements must be electrically short (at least at the longer wavelengths) so their antenna pattern will be that of a short dipole. A vertical short dipole, sensitive to the perpendicular component of the electric field, has a null at the zenith and is therefore of limited use in synthesis mapping.

If we consider a short (Hertzian) dipole parallel and close to the surface of the Moon, relative permittivity ϵ_{r}, the image dipole seen beneath the regolith is $-(\epsilon_{\mathrm{r}}-1)/(\epsilon_{\mathrm{r}}+1)$ times the real dipole in the vacuum (ignoring the imaginary component of the relative permittivity for the moment). Taking the relative permittivity of the Moon to be about 6, this image reduces the total gain in the vacuum direction to about $2/(\epsilon_{\mathrm{r}}+1) = 2/7$ its free-space value (Figure 6). Similarly, the gain beneath the surface is increased by a factor of about$(\epsilon_{\mathrm{r}}+3)/(\epsilon_{\mathrm{r}}+1) = 9/7$.

The question of sensitivity will be considered later, but it is important to note at this point that, if all the system noise arises from the sky, it is the *directivity* of the antenna, rather than the gain, that determines sensitivity. Here we define gain as a measure of the power delivered into a matched load as a function of direction whereas directivity is a measure of the angular extent of the antenna beam on the sky. Hence all short dipoles in free space, matched or not, have the same directivity. Their gain on the other hand will depend on proper matching. Gain therefore has the same effect on both the signal and the noise and a change in gain will not affect the signal-to-noise ratio. The directivity determines the proportion of the field-of-view occupied by the signal source (as opposed to the noise source) and hence directly affects the signal-to-noise ratio of the instrument. This simplification breaks down when the noise from the front-end amplifiers is comparable with the voltages they are to amplify. This will occur when the forward gain of the antenna drops below some level defined by the amplifier characteristics. It seems

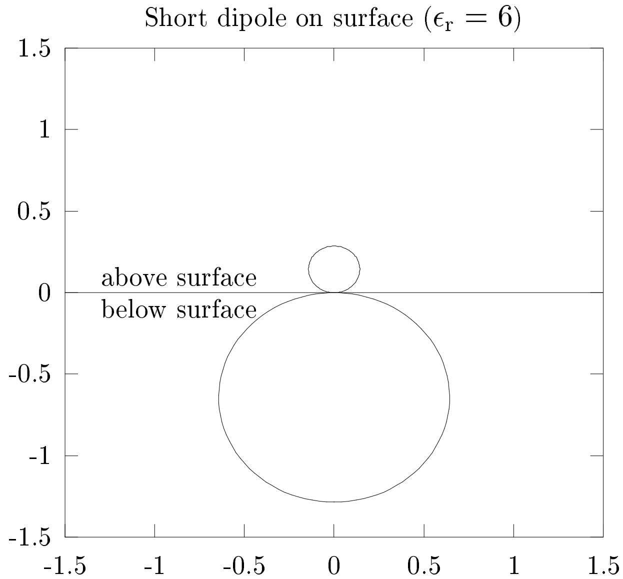

Figure 6: Relative directivity of a short dipole placed horizontally on the surface of the Moon ($\epsilon_r = 6$).

however that a short dipole placed on the lunar surface suffers a drop in forward gain of only about 5 dB, which should be insufficient to bring the signal down to this threshold level in any practical system.

As noted above, the lobe of the dipole antenna pattern directed into the Moon is stronger than the upward lobe. This is important because any strong signals reflected from discontinuities beneath the lunar surface could be picked up by this lobe and confuse the sky observations. The relevant electrical property of the regolith to consider here is its loss tangent, L, defined as the ratio of the imaginary to the real part of its complex relative permittivity. The loss tangent, measured at between 0.001 and 0.1 during the Apollo missions [5], gives us the skin-depth of the Moon,

$$\frac{D_s}{\lambda} = \frac{1}{\pi L \sqrt{\epsilon_r}}, \tag{19}$$

and hence the depth at which reflections become negligible. The skin depth, D_s, is therefore between about 1–100 wavelengths. This range allows for propagation over significant distances, particularly at the lowest frequencies, so the site should be chosen carefully to minimise the effects of sub-surface reflections.

5 Telescope design for an all-sky survey

At frequencies > 400 MHz telescopes are usually designed either as survey instruments, able to cover a significant fraction of the sky at low resolution, or as high resolution instruments to be directed at specific sources. At lower frequencies the diffraction limit makes it progressively harder to construct high resolution instruments and so most telescopes operating below about 150 MHz are designed to carry out surveys. At frequencies below 10 MHz the limitations imposed by scattering in the ISM and IPM become the dominant effect, and high resolution imaging becomes impossible. A lunar low-frequency array would therefore be a survey instrument. The scattering limit is such that resolutions of a few tens of arcminutes are desirable. Furthermore, the sky background is both the dominant noise source and the primary target for mapping, so the temperature sensitivity will usually be good.

With these points in mind we should now consider the technical issues that affect the telescope design.

5.1 Phased array or interferometer?

One of the more fundamental design choices that must be made is whether the telescope should be a phased array of dipole elements, raster-scanning the sky beam-by-beam to build up a survey map, or an interferometer, measuring spatial scales over a large fraction of the sky all at once. Both approaches have their advantages and disadvantages, although it must be said that on Earth most low-frequency surveys are carried out with interferometers (such as the CLFST in Cambridge, UK).

The data rate to the Earth from a phased array can be made very low, as some integration can be done on the Moon. A similarly low rate from an interferometer requires the correlator to be either on the Moon's surface or in close orbit. A phased array also has slightly better sensitivity than an interferometer, but it is basically a power-measuring telescope, so interference always adds positively, no matter where it is in the beam. An interferometer on the other hand is less sensitive to interference, particularly if the source moves through the beam, as the signals add either positively or negatively, depending on the sign of the lobe the source is in. In both cases the beams rotate on the sky over long integration periods. However the mean sidelobe levels of a phased array, averaged over the rotation, are those of the mean square voltage pattern, whereas an interferometer gives the square of the mean voltage pattern. We can therefore expect the sidelobes to be lower in a map made with an interferometer.

Conventionally, both phased arrays and interferometers need path compensation. This represents one of the more difficult design features to implement electronically in any telescope as the delays involved are often very small (∼nanoseconds). On Earth these delays are usually generated by inserting appropriate lengths of cable into the signal path. On the Moon this solution is unattractive, as the weight of the cabling needed would be prohibitive. We can however remove the need for path compensation if we work with sufficiently narrow bandwidths. In this way the 'white light' fringe condition is maintained naturally. Roughly, if we wish to map a region of sky of angular width θ_v using a baseline (or array size) of L without path compensation, the bandwidth used must be

$$\Delta\nu < \frac{c}{L\theta_\mathrm{v}} . \tag{20}$$

A practical scheme would involve dividing up the total observing bandwidth at each antenna into many narrow sub-bands (see below), probably by using digital signal processing chips. The antenna sub-bands are then either summed with the correct phase to point the telescope in the desired direction (phased array) or separately correlated to produce many narrow-band maps which can be co-added (interferometer).

This scheme falls more naturally into an interferometer design, which already requires considerable digital processing, than into a phased array design, which is potentially less reliant on digital techniques. However, to get the *full* benefit of a phased array telescope, one would have to generate many phased beams on the sky simultaneously (so generating the equivalent of a focal-plane array at the focus of big dish). This would itself require a considerable amount of Moon-based electronics so the apparent simplicity of the phased-array approach is lost.

Interstellar temporal broadening is sufficiently great for there to be essentially no source variability at these frequencies, so the time needed for synthetic aperture interferometric mapping need not be a limitation. Furthermore, if we put the correlator on the Moon or in lunar orbit the high data-rate from an interferometer ceases to be an issue and the post-correlation data rate can be made as low as that from a phased array.

It should be noted that the digital design for the telescope as outlined above is sufficiently flexible for the decision between the two competing designs to be one made in the DSP software rather than the telescope hardware. To avoid the need for path compensation, both designs require the signals from each antenna to mixed to baseband, digitised and then split into many sub-bands by an FFT chip. These sub-bands are then passed to a DSP block, situated close to the centroid of the antennas, which combines the digital signals to produce beams on the sky that are either 'point-like' (the phase array) or 'wave-like' (the interferometer). The distinction is not as severe as it seems at first. Probably the most important distinction between the two appears only when we consider the rotation of the Moon and the effect of this rotation on the mean beamshape. The beamshape is better when we configure the telescope as an interferometer, so from this point onward we will consider only the needs of the interferometer.

5.2 Field-of-view considerations

The telescope's field-of-view is limited by the presence of the Moon cutting out approximately 2π steradians of sky at any one time. The receiving elements themselves are electrically short. Although they carry a dipole anisotropy they will receive signals from practically all the visible sky simultaneously. As described above, the field of view of the whole telescope is therefore defined by chromatic effects. For an interferometer this is known as 'bandwidth smearing', and is caused by the dependence on wavelength of both the resolution and size of the map. Loosely, Equation (20) shows that to make an $n \times n$ pixel map the fractional bandwidth used must be

$$\frac{\Delta\nu}{\nu} \leq \frac{1}{n}. \tag{21}$$

To take an example, a synthesis map made by a telescope on the Moon's equator covering the whole sky with a resolution of 0.25 degrees would have a value of $n \simeq 800$. If the observing frequency were 1 MHz, the bandwidth of each sub-channel would therefore have to be $\sim$ 1 kHz. This would mean that a map of the sky made at 1 MHz with a total bandwidth of 100 kHz would in fact consist of about 100 narrow-band maps added together. In practice, this addition occurs most naturally in the aperture plane immediately after correlation and before the final mapping transform.

5.3 Processing power

As will be shown below the lunar telescope will need about 300 elements but will have an instantaneous bandwidth of only about 100 kHz. The total data rate is therefore high, but it is distributed over many channels. This allows us to consider a fully digital design for the correlator. As has already been stated, path compensation can be side-stepped if the data from each antenna are divided into a great many ($\sim$ 100) sub-bands before correlation. This can best be done digitally using specific FFT chips or more general digital signal processing (DSP) chips. Once digitised, the correlation is then naturally carried out digitally. The amount of processing power required to handle all the data from the telescope must therefore be estimated. Assuming there are 300 elements in the interferometer, each measuring two polarisations (possibly the worst case), the number of real correlations to be carried out in each band is

$$\begin{aligned} N_{\mathrm{corr}} &= \underbrace{\frac{1}{2}\times 300\times 299}_{\text{No. of baselines}} \times \overbrace{2}^{\sin\ \&\ \cos} \times \underbrace{2}_{\text{polarisations (?)}} \\ &= 179,400\,. \end{aligned}$$

In terms of the number of floating point operations per second (flops) there is no overhead in dividing the full bandwidth into many sub-bands because the data rate in each is proportionately less. If we assume a full bandwidth of 100 kHz, the processing power necessary to correlate all available baselines is therefore about 3.6×10^{10} flops. Although this appears a fearsome figure, the task can be distributed efficiently between a number of processors. Even with present day technology, using chips from the inexpensive Analog Devices ADSP2100 family, an array of about 1000 processors would be sufficient.

5.4 Flux sensitivity

The telescope can be used to detect unresolved or resolved sources. The sensitivity of the instrument to radiation from an unresolved source is defined by its flux sensitivity. The sensitivity to a resolved source (i.e., a source larger than the synthesized beam) is defined by its brightness temperature sensitivity, or flux sensitivity per unit solid angle.

In both cases the noise that limits the sensitivity should be dominated by emission from the sky, which is at temperatures of up to 10^7 K at these frequencies†, rather than the receiver electronics. This is an important design criterion for the dipole/front-end sub-system. The radiation resistance of a short dipole is about

$$R_{\mathrm{r}} \simeq 20\pi^2 l^2/\lambda^2\,, \tag{22}$$

so at 1 MHz a 10 m antenna has a radiation resistance of 0.2 Ω. Matching to such a small resistance is difficult but can be overcome if we realise that, as both the noise and the signal come from the antenna, there is no need for efficient power transfer between the antenna and the preamplifier. The preamplifier can therefore have a high input impedance so that the antenna

†The sky brightness is about 12 Jy per $1/4\times 1/4$ degree beam at 1 MHz

simply acts as a probe of the electric field, developing a potential difference over its ends of $V \simeq El$ where E is the electric field and l the length of the dipole. Assuming this voltage can be amplified without introducing further noise the telescope will see a 'bright' sky, the brightness of which will vary somewhat from point to point. It is this brightness variation, caused by differences in both synchrotron emission and interstellar absorption, that the telescope must map. Discrete sources will be seen within this brightness distribution so measurement of individual flux densities will be contaminated by uncertainties in the point-to-point variance of background emission.

Because the noise contribution is 'self-noise' from the structures we wish to map, the sensitivity of the instrument is very high. Indeed, if we were to use a fully-filled phased array, the signal-to-noise ratio per beam area would be

$$\textsc{snr} = \sqrt{\Delta\nu\tau}\,, \tag{23}$$

where $\Delta\nu$ is the full bandwidth and τ the integration time per beam. A multi-beam array covering the whole sky to the desired resolution would therefore reach a signal-to-noise ratio of 100 with a bandwidth of 100 kHz in 0.1 seconds! More realistically, we cannot attain a resolution of 0.25 degrees with a fully filled aperture as the number of individual elements would be prohibitively high, so the sensitivity will be correspondingly lower.

Generally, the flux sensitivity of an n element interferometer ($n \gg 1$) is

$$\Delta S = \frac{2kT_{\rm sys}}{nA_{\rm eff}\sqrt{\Delta\nu\tau}}\,, \tag{24}$$

where $A_{\rm eff}$ is the effective area of a single element, $T_{\rm sys}$ the system temperature, $\Delta\nu$ the total observing bandwidth and τ the observing period. The effective area in this expression represents the directivity of the antenna elements. For a short dipole

$$A_{\rm eff} = \frac{3}{2}\frac{\lambda^2}{4\pi} \tag{25}$$

so the flux sensitivity of the interferometer is

$$\Delta S = \frac{16kT_{\rm sys}}{3n\lambda^2\sqrt{\Delta\nu\tau}}\,. \tag{26}$$

A power-law fit to to the galactic spectrum seen by RAE below 4 MHz gives $T_{\rm sys} = 10750\lambda^{1.324}$. The flux sensitivity in janskys then becomes

$$\Delta S_{\rm Jy} = 5.3 \times 10^6\,\frac{\nu_{MHz}^{0.676}}{n\sqrt{\Delta\nu\tau}}\,. \tag{27}$$

As an example, taking $n = 300$, $\Delta\nu = 10^5$ Hz and $\tau = 1.3 \times 10^6$ seconds (15 days) the flux sensitivity is 0.05 Jy. Although probably insufficient to detect emissions from an extra-solar-system planet, this sensitivity is sufficient to map the sky background (which at 1 MHz has a surface brightness of about 12 Jy beam^{-1} at a resolution of 0.25 degrees) with a signal-to-noise ratio of about 200. This is effectively the temperature sensitivity of the telescope—a result that will now be demonstrated more directly.

5.5 Temperature sensitivity

The temperature sensitivity of the telescope is of greater importance than its flux sensitivity. This is because the resolution of the instrument will be at or slightly below the angular broadening limit set by scattering, and most of the observations will therefore be of 'resolved' structures, broadened to more than one pixel.

The temperature sensitivity can be derived directly from the flux sensitivity, defined by Equation (26). The flux density from a region of the sky of solid angle Ω and temperature T is defined as

$$S = 2kT\Omega/\lambda^2 \,. \tag{28}$$

If the sky is imaged with a maximum baseline of D, then $\Omega \simeq (D/\lambda)^2$. Combining this with the previous equation and Equation (26) gives a temperature sensitivity of

$$\Delta T = \frac{D^2 T_{\rm sys}}{n A_{\rm eff} \sqrt{\Delta\nu\tau}} \,, \tag{29}$$

and a signal-to-noise ratio in temperature of

$$\text{SNR} = \frac{T_{\rm sys}}{\Delta T} = f\sqrt{\Delta\nu\tau} \,. \tag{30}$$

The factor f equals $nA_{\rm eff}/D^2$ and is the *filling factor* of the interferometer—literally the fraction of the the synthesised aperture actually filled by real antennas at any one moment. It is this factor that drops the temperature sensitivity well below the theoretical figure derived for a fully-filled aperture at the beginning of this section. If we take $n = 300$, $\nu = 1$ MHz and D = 70 km (0.25 degree resolution) we get $f \simeq 6.6 \times 10^{-4}$. Clearly most of our aperture is missing. The temperature signal-to-noise ratio after a 15-day integration at 1 MHz with a bandwidth of 100 kHz is therefore about 200.

A signal-to-noise ratio of 200 is quite sufficient to do most of the astronomy we require. Indeed, uncertainties in the sidelobe levels may prevent useful observations being made with greater finesse than this. Thus a 300-element interferometer operating at 1 MHz placed near the lunar equator can map the entire visible sky by rotation aperture synthesis in half a lunar day. A practical observing program would involve many such maps being made at spot frequencies throughout the design frequency range of the instrument.

The filling factor for short dipoles scales as λ^2, so that at 10 MHz it is 100 times less than at 1 MHz. The system described above would therefore have a signal-to-noise ratio of only 2 at 10 MHz—insufficient for practical work. This figure may be improved by

- Only using an inner 'sub-array' for the higher frequencies. This array would need to have fewer antennas but a larger filling factor. The angular resolution would then be limited to less than that available with a 70 km baseline (1.5 arcmin) but the temperature sensitivity would recover.
- Increasing the observing bandwidth at the higher frequency.
- Observing the sky for more than one night.

Part of the solution to this problem is therefore to be found in optimally positioning the antennas.

5.6 Relative antenna positions

The subject of antenna placement is a particularly subtle part of any interferometer design. In the case of the VLFA it is further complicated by the need for a wide range of operating frequencies and the strong dependence of filling factor (and hence sensitivity) on wavelength described above. The optimum solution must wait for its own design study, but some general points can be made straightaway.

The individual antennas in the instrument are dipoles and respond well to signals from practically anywhere on the sky. These elements have no real primary beam so strong sources are limited only by the synthesised beam, the sidelobes of which should be kept as low as possible. For a fixed number of antennas, the power in these sidelobes is minimised when the baselines are non-redundant, making a non-redundant configuration particularly attractive.

To continue the design, two conflicting criteria must be balanced:

1. The quality of the map is improved if the interferometer samples the transform plane uniformly, so measuring all spatial scales in the sky brightness distribution.

2. The temperature sensitivity of the telescope depends on the filling factor, which, because we are using short dipoles, drops as λ^2. We can only recover sensitivity at the higher frequencies (and the same resolution) if the filling factor for the shorter baselines is greater than that for the larger baselines.

Some of the antennas must contribute only to the larger spacings so they can be excluded at higher frequencies. This makes the array smaller, and allows us to attain at higher frequencies a filling factor similar to that attainable at lower frequencies. Clearly, the antennas cannot be arranged with uniform density as this would not allow us to improve the filling factor by excluding the outer ones. Rather, the space-density of the antennas must drop off, possibly rapidly, as we move out from the centre. This introduces a notional 'inner' and 'outer' array into the design. The two arrays are used together in the lower portion of the frequency range to get maximum resolution. The outer array, containing fewer antennas, is not used for higher frequency observations. At these frequencies the inner array alone has a better filling factor and can map the sky at a similar resolution.

The classic 'Y'-shaped design, used for the VLA and other telescopes, embodies many of these features. The antennas are spaced logarithmically along the three arms such that the distance to the ith antenna is proportional to i^α ($\alpha \geq 1$). In this way, spatial scales are measured similarly over a wide range of observing frequencies, and the filling factor for the inner antennas alone is greater than of the whole.

It is difficult to use a simple 'Y'-shaped design for the VLFA because, with 300 antennas in total, there is insufficient space in the inner zone. A practical design would include antennas spread more evenly around the vertical axis of the array in this inner zone, resolving to a classic 'Y' only in the more distant reaches.

If there are n antennas in total, we can define an antenna density function by

$$\rho(\boldsymbol{r}) = A_{\rm eff} \sum_{i=1}^{n} \delta(\boldsymbol{r} - \boldsymbol{r}_i)\,, \tag{31}$$

where $\boldsymbol{r}_i$ is the position vector of the ith antenna relative to the telescope centre. The filling factor of the array, out to a distance R from the centre, is then

$$f(R) = \frac{A_{\rm eff} \int^{|\boldsymbol{r}|\leq R} \rho(\boldsymbol{r})\, d^2 r}{\pi R^2}\,. \tag{32}$$

We can now compare the sensitivity of the instrument at different frequencies by fixing the resolution at $\theta_{\rm r}$ and only using antannas out to $R = \lambda/(2\theta_{\rm r})$.

Taking $A_{\text{eff}} = 3\pi\lambda^2/8$ gives a total filling factor as a function of wavelength of

$$f_\lambda = \frac{3}{2}\theta_{\text{r}}^2 \int^{|\boldsymbol{r}|\leq\lambda/(2\theta_{\text{r}})} \rho(\boldsymbol{r})\, d^2r\,. \tag{33}$$

The optimal positions of the antennas, $\{\boldsymbol{r}_i\}$, are the ones that maximise the above expression and minimise the power in sidelobes of the synthesised beam over the design frequency range[‡]. The calculation must also take account of the relative proximity of antennas. If closer than about a wavelength they do not contribute independently to the filling factor and must be taken together. The procedure is not trivial, but the optimisation strategy is well defined.

5.7 Summary of the telescope design

When mapping the sky at these frequencies we may assume that the system temperature is due solely to the noise arriving in through the antenna. We can therefore ignore noise contributions from the electronics themselves. The design of the front-end is crucial, as an insensitive design may result in the receiver temperature exceeding the contribution from the sky, so disallowing this assumption.

The resolution of the sky survey is limited by scattering to a few tens of arcminutes, so it is more useful to think in terms of brightness temperature sensitivity (i.e., a measure of flux per unit solid angle) than flux sensitivity. All the system noise is assumed to be due to the sky, so the expression for the signal-to-noise ratio in the map is particularly simple, and reduces to

$$\text{SNR} = f\sqrt{\Delta\nu\tau}, \tag{34}$$

where $\Delta\nu$ is the observing bandwidth, τ the integration time and f the filling factor of the synthesis array. The filling factor is defined as the ratio of the total physical collecting area of the elements to the area of the synthesised aperture. Taking the maximum baseline of the array to be D, the synthesised aperture has an area of $\simeq D^2$. If we assume the receiving elements are electrically short dipoles spaced sufficiently far apart that they do not interfere with each other (i.e., $> \lambda$) they each have an effective collecting area of

$$A_{\text{dipole}} = \frac{3}{2}\frac{\lambda^2}{4\pi}. \tag{35}$$

It is helpful to note that the concept of 'collecting area' is used here to reflect the extent of the beam pattern on the sky rather than the efficiency of the

[‡]the instantaneous synthesised beam is the Fourier transform of the autocorrelation of $\rho(\boldsymbol{r})$.

antenna at absorbing energy. The ratio of these two areas gives the filling factor

$$f = n\frac{3}{8\pi}\left(\frac{\lambda}{D}\right)^2, \tag{36}$$

where n is the number of dipole elements deployed in the array.

Finally therefore, the signal-to-noise ratio for the telescope becomes

$$\text{SNR} = n\frac{3}{8\pi}\frac{\lambda^2}{D^2}\sqrt{\Delta\nu\tau}. \tag{37}$$

If we take as an example $\lambda = 300$ m (1 MHz), $\Delta\nu = 100$ kHz, $\tau = 1.2 \times 10^6$ sec (14 days) and $D = 70$ km we get a signal-to-noise ratio of snr $\simeq 0.76n$. A choice of $n = 300$ therefore results in a perfectly acceptable signal-to-noise ratio of 228.

The all-sky survey could therefore be completed in one lunar night. Any proper survey would then go on to repeat the measurements at a number of spot frequencies throughout the design range of the telescope. A suitable number might be 20 frequencies, spaced logarithmically between 0.5 and 10 MHz.

It is important to consider how the n antennas are to be arranged within the boundary of the synthesised aperture. Clearly, the best filling factors are achieved when the elements are in a close-packed configuration, literally 'filling' the synthesised aperture. In the case of the VLFA though, there are insufficient antennas to achieve this, and other configurations must be considered. Arrangements that perform well in 'snap-shot' mode are of lesser interest as the instrument will almost always be operating as a rotation synthesis telescope. A classic 'Y'-shaped configuration is attractive, with further antennas placed around the centre to increase the inner filling factor. The filling factor of the telescope taken as a whole drops as ν^{-2}, so at higher frequencies this 'inner' array can be used on its own without reducing the angular resolution below the level attainable at lower frequencies.

6 Overall summary

We see from the above that there are a number of important effects that must be considered and balanced in the design of a lunar radio telescope operating at very low frequencies. One of the driving forces behind such a telescope is the need to get above the Earth's own ionosphere, which is largely opaque to radio waves at frequencies below 10 MHz. What we are left to contend with is a residual lunar ionosphere, which has a plasma frequency well below 0.5

MHz during the lunar night, the interplanetary medium and the interstellar medium.

The lunar ionosphere can be neglected if we observe only when the Sun is below the horizon, but the IPM and ISM will always be present. Their main effect is to broaden the apparent angular sizes of sources to discs of around 1 degree at 1 MHz, so limiting the effective angular resolution of the instrument. Although it may be possible to remove some of the effects of the IPM using scintillation techniques those from the ISM are irreversible.

The scattering also limits the temporal resolution of the instrument. This is severe enough for it to be impossible to detect pulsed emission from nearly all known pulsars and to reduce the instruments sensitivity to transient signals ($\lesssim 1$ s) in the solar system at frequencies below 600 kHz.

One of the clearest signatures we expect to see with the VLFA is that of free-free absorption in the ISM. This has the effect of dimming both the synchrotron background radiation and signals from discrete sources. The amount of extinction in a particular direction depends on the emission measure and this will vary both within the galactic plane and out of it. At frequencies below 1–2 MHz we can expect the sky to appear almost uniformly foggy. At higher frequencies the absorption will give the background emission a more 'blotchy' appearance. The study of these effects gives important information on both the ISM and the Galaxy's synchrotron background radiation and is a primary goal of the mission.

The antennas themselves will be electrically short ($l \ll \lambda$) and can be laid flat on the Moon's surface. This skews the gain pattern so that the antennas are more sensitive to signals coming up from beneath the surface, but careful placement should ensure that nearly all the signal received comes directly from the sky.

The antennas must be arranged in a fixed configuration giving good sensitivity over a wide range in frequencies. The most promising type of design appears to be one similar to the classic 'Y' shape but with extra antennas in the inner zone to increase the filling factor there. Such an instrument, operated as an interferometer, should have sufficient temperature sensitivity to map the whole sky with a resolution of 0.25 degrees in half a lunar day, assuming a bandwidth of 100 kHz. The correlator used for this should be digital in design and make heavy use of DSP techniques. In particular, by dividing the observing bandwidth into many narrower sub-bands the need for path compensation can be removed.

References

[1] Cordes, J.M., Pidwerbetsky, A., & Lovelace, R.V., 1986, *Ap. J.*, **310**, 737.

[2] Cordes, J.M., 1990, *Low Frequency Astrophysics from Space*, eds. Kassim, N.E., & Weiler, K.W., Springer Verlag Lecture Notes in Physics No. 362, p. 165.

[3] Cornwell, T.J., & Napier, P.J., 1986, *Radio Astronomy from Space*, ed. Weiler, K.W., Proc. of NRAO Workshop No. 18, p. 215.

[4] Erickson, W.C., 1964, *Ap. J.*, **139**, 1290.

[5] Heiken, G.H., Vaniman, D.T., & Bevan, M.F., 1991, eds., *The Lunar Source Book*, Cambridge University Press, p. 40.

[6] Novaco, J.C., & Brown, L.W., 1978, *Ap. J.*, **221**, 114.

[7] Reynolds, R.J., 1990, *Low Frequency Astrophysics from Space*, eds. Kassim, N.E., & Weiler, K.W., Springer Verlag Lecture Notes in Physics No. 362, p. 121.

[8] Rickett, B.J., 1977, *Ann. Rev. Astron. Astrophys.*, **15**, 147.

[9] Savich, N.A., 1976, *Space Research XVI*; Proc. of Open Meetings of Workshop Groups on Physical Sciences, Akademie-Verlag, p. 941.

[10] Tribble, P.C., 1991, *Mon. Not. R. Astr. Soc.*, **250**, 726.

[11] Vyshov, A.S., 1976, *Space Research XVI*; Proc. of Open Meetings of Workshop Groups on Physical Sciences, Akademie-Verlag, p 945.

[12] Vyshov, A.S., & Savich, N.A., 1979, *Cosmic Research*, **16**, 450.